Letter

CH₃NH₃PbCl₃ Single Crystals: Inverse Temperature Crystallization and Visible-Blind UV-Photodetector

Giacomo Maculan,[†,∥] Arif D. Sheikh,[‡,∥] Ahmed L. Abdelhady,[†,§] Makhsud I. Saidaminov,[†] Md Azimul Haque,[‡] Banavoth Murali,[†] Erkki Alarousu,[†] Omar F. Mohammed,[†] Tom Wu,*[,‡] and Osman M. Bakr*[,†]

[†]Division of Physical Sciences and Engineering, Solar and Photovoltaics Engineering Research Center, King Abdullah University of Science and Technology (KAUST), Thuwal 23955-6900, Kingdom of Saudi Arabia

[‡]Materials Science and Engineering, King Abdullah University of Science and Technology (KAUST), Thuwal 23955-6900, Kingdom of Saudi Arabia

[§]Department of Chemistry, Faculty of Science, Mansoura University, Mansoura, 35516, Egypt

S Supporting Information

ABSTRACT: Single crystals of hybrid perovskites have shown remarkably improved physical properties compared to their polycrystalline film counterparts, underscoring their importance in the further development of advanced semiconductor devices. Here we present a new method of growing sizable CH₃NH₃PbCl₃ single crystals based on the retrograde solubility behavior of hybrid perovskites. We show, for the first time, the energy band structure, charge recombination, and transport properties of CH₃NH₃PbCl₃ single crystals. These crystals exhibit trap-state density, charge carrier concentration, mobility, and diffusion length comparable with the best quality crystals of methylammonium lead iodide or bromide perovskites reported so far. The high quality of the crystal along with its suitable optical band gap enabled us to build an efficient visible-blind UV-photodetector, demonstrating its potential in optoelectronic applications.
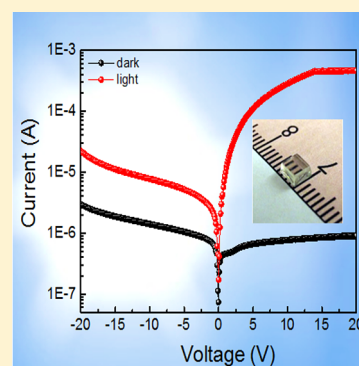
In the past few years, organo-lead halide perovskites MAPbX₃ (MA = CH₃NH₃⁺, X = Cl⁻, Br⁻, or I⁻) have drawn the attention of many scientists due to their attractive optical and electrical properties, together with their moderate cost and low-temperature solution-processability.[1−7] These merits make them one of the most promising candidates for the industrial development of next-generation optoelectronic devices. In particular, MAPbI₃ and MAPbBr₃ showed strong optical absorption coefficients across the visible spectra,[8] combined with balanced and long-range electron−hole diffusion lengths[9] and low trap-state densities,[10,11] resulting in broad employment of these materials in high efficiency solar cells,[12−17] light emitting diodes,[18,19] lasers[20,21] and photodetectors.[22−24]

Optical and electrical studies conducted on single crystals of organo-lead bromide and iodide perovskites[11,25] revealed that the properties are considerably enhanced in single crystals, compared to their polycrystalline thin film counterparts. This property enhancement is reflected by the absence of an absorption peak near the band gap of the crystals, which indicates more order and long-range structure.[11] Moreover, charge carrier lifetimes in single crystals are longer due to a lower trap-induced recombination rate (357 ns for MAPbBr₃ single crystal and 168 ns for the polycrystalline thin films).[11] In terms of diffusion length, it was reported that there was a 2 orders of magnitude increase from 1 μm (films) to 175 μm (crystals).[25] Hence, the growth of MAPbX₃ crystals from

solution is of key importance toward the advancement of perovskite-based applications.

Very recently we have reported the fast solution-based crystal growth of MAPbI₃ and MAPbBr₃ by inverse temperature crystallization (ITC),[26] overcoming the time-consuming conventional crystallization methods such as the typical cooling[27] or antisolvent vapor-assisted crystallization techniques.[11] The optical and transport properties of these ITC grown crystals were comparable to the crystals grown over a much longer period of time.

However, for MAPbCl₃ single crystals grown by the traditional crystallization techniques,[28,29] only structural characterization was carried out, showing the temperature-dependent phase transitions of the material,[29−31] while the electrical characterization was limited to the phase-dependent dielectric permittivity investigation.[28,29] Moreover, to date, optical absorption and emission spectra of MAPbCl₃ single crystals have not been reported. Exploring the optical and electrical properties of the wide band gap MAPbCl₃ single crystal may provide a better understanding of the chloride-based perovskite in the development of optoelectronic devices, in particular, visible-blind UV-detectors.
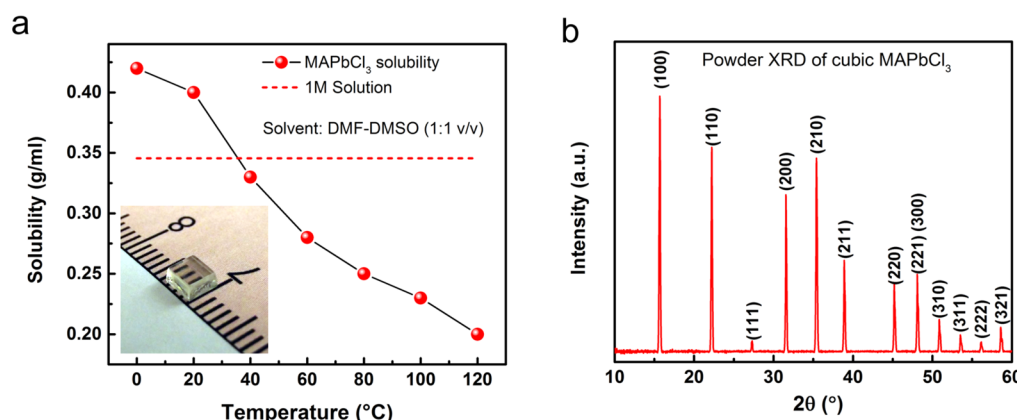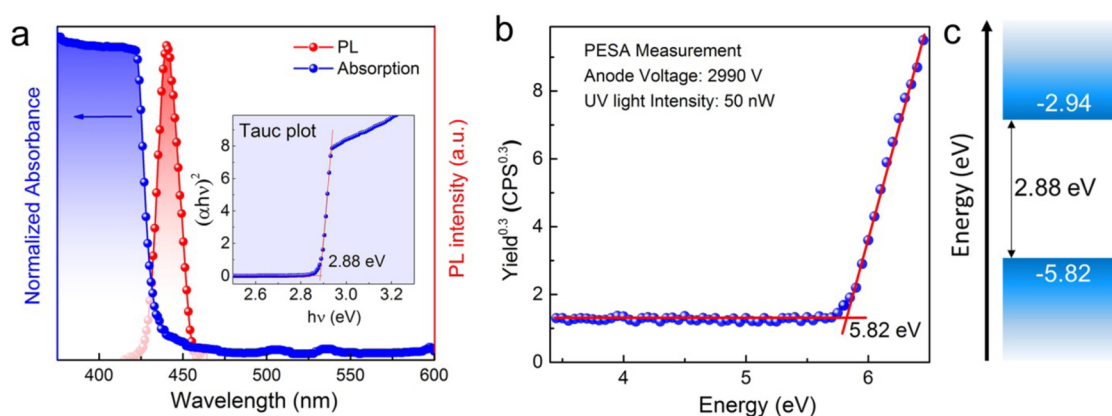
Figure 1. (a) Solubility data for MAPbCl₃ powder in DMSO−DMF (1:1 v/v) at different temperatures, showing the monotonic decrease of solubility from (0.40 ± 0.05) g/mL at room temperature, to (0.20 ± 0.05) g/mL at 120 °C. Inset: Transparent single crystal grown from MAPbCl₃ solution in DMSO−DMF (1:1 v/v) after 48 h in an oil bath at 50 °C. (b) PXRD pattern of ground MAPbCl₃ crystal.

Figure 2. (a) Absorption and PL spectra of MAPbCl₃ single crystal, which reveals an absorption edge at 435 nm and determines the optical band gap to be 2.88 eV (inset). Excitation wavelength of 294 nm was used to record the PL. (b) PESA measurement showing the level of the valence band at −5.82 eV. (c) VBM and CBM of MAPbCl₃ single crystals. Energy levels are expressed using the electron energy in vacuum as a reference.

We report here the ITC of MAPbCl₃ through selecting an appropriate solvent mixture. We investigated the electrical and optical properties to estimate, for the first time, the energy band levels and a number of important semiconducting figures of merit such as charge carrier mobility, exciton lifetime and diffusion length. All these parameters are essential for the utilization of this material in practical applications. Furthermore, we exploited the optical and charge-transport properties of MAPbCl₃ single crystals to design the first UV-photodetector based on organo-lead chloride perovskite single crystal, with high ON-OFF current ratio, fast photoresponse, and long-term photostability.

High purity along with minimum structural defects are well-known to be key factors for the successful application of semiconductors in optoelectronic devices.[32] To this end, particular attention was paid to the synthesis and solution growth process, primarily, to the choice of the solvent. We made several attempts trying to form 1 M solution of the precursors by dissolving stoichiometric amounts of MACl and PbCl₂ in different solvents; we figured out that while the mixture of the two precursors were likely to dissolve in dimethyl sulfoxide (DMSO), without showing any retrograde solubility, only small amount of precursors dissolved in N,N-dimethylformamide (DMF). We hypothesized that a mixture of DMSO and DMF might initiate the retrograde solubility behavior of MAPbCl₃. Accordingly, highly concentrated

solution (1M) of the precursors with retrograde solubility behavior was achieved through balancing the ratio of DMF to DMSO.

Figure 1a shows the solubility of MAPbCl₃ powder in a mixture of DMSO−DMF (1:1 v/v), clearly demonstrating the decrease of solubility at elevated temperatures. Next, we optimized the crystallization temperature and precursor concentration to form only a few nuclei/crystals. The optimized synthesis and growth processes as well as the solubility test procedure are described in detail in the Supporting Information. Inset of Figure 1a shows a highly transparent and colorless MAPbCl₃ crystal grown by ITC, with a parallelepiped shape and typical dimensions of 2 × 4 × 4 mm³. Powder X-ray diffraction (PXRD) of the ground crystal confirmed pure single-phase of cubic MAPbCl₃ perovskite (Figure 1b) with lattice constant *a* = 5.67 Å, showing consistency with the previously reported PXRD data of the same single crystals obtained through the conventional crystallization technique.[33]

Further, we studied optical properties of the MAPbCl₃ crystal. Crystals exhibit a sharp absorption edge at 435 nm and photoluminescence (PL) peak at 440 nm (Figure 2a), notably red-shifted compared to MAPbCl₃ thin films, which show optical absorption edge at 399 nm and PL peak at 408 nm.[34] These findings are in good agreement with recent studies on MAPbBr₃ and MAPbI₃, where single crystalline samples
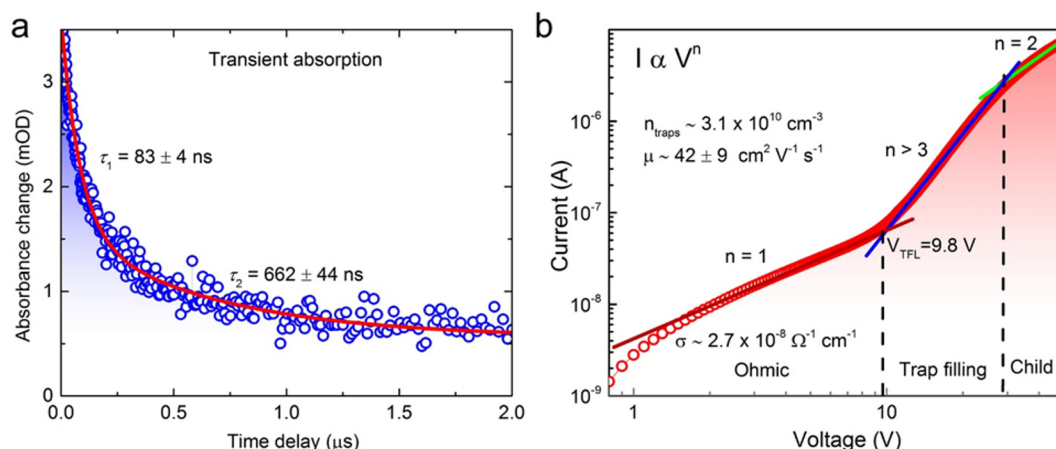
Figure 3. (a) Transient absorption in MAPbCl$_3$, showing a fast component decay time of (83 ± 4) ns and a slow component of (662 ± 44) ns. The monitoring wavelength of the TA kinetics is 600 nm. (b) Current−voltage response of MAPbCl$_3$ single crystal, which shows three different regions: a linear ohmic regime ($I \alpha V$, red line) is found at lower voltages. V_{TFL} ($= 9.8$ V) marks the transition into the trap-filled limit ($I \alpha V^{n>3}$, blue line) which is followed by the Child's regime ($I \alpha V^2$, green line) at higher voltages.
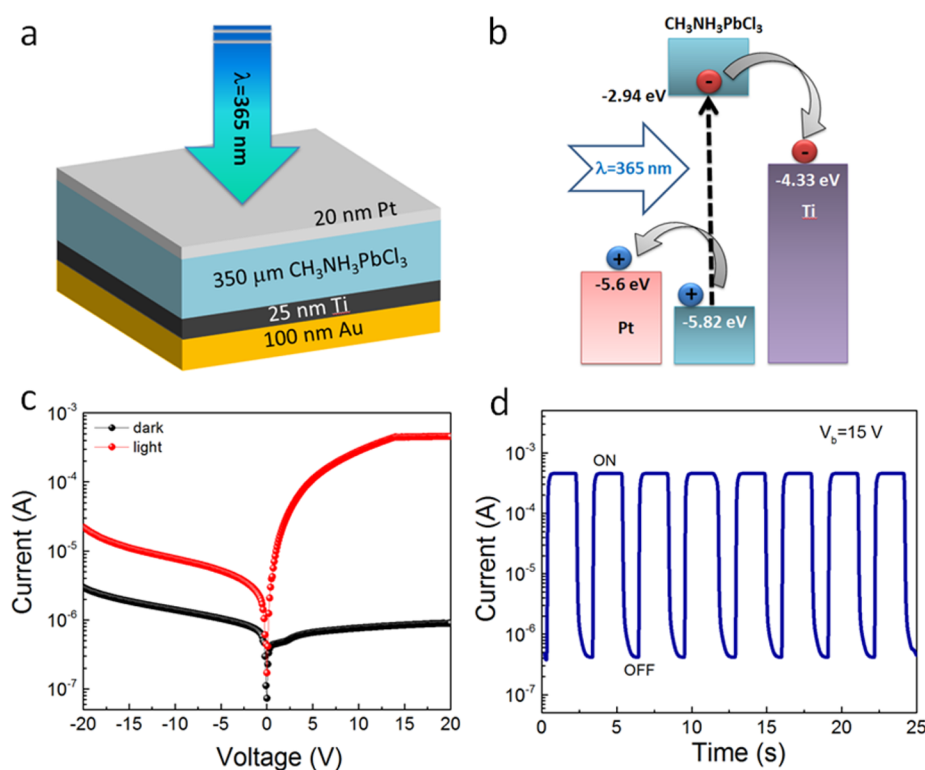

Figure 4. (a) Device architecture of the MAPbCl$_3$ single-crystal-based photodetector. (b) Energy band diagram. (c) Photo and dark current−voltage (I−V) curves of the photodetector under illumination with solar-blind UV light ($\lambda = 365$ nm). (d) ON−OFF photoresponse at a bias voltage of 15 V under modulated UV illumination.

possess a narrower band gap and a subsequent red-shifted PL peak, compared to their thin film counterparts, suggesting lower trap densities due to a higher-dimensional structurally coherent units that are more tight in the single crystal compared to their polycrystalline counterparts, while the low-dimensional units, which could be present in thin films are known to emit at lower wavelength.[11] In addition it has been reported that larger crystallite size results in red-shifted PL.[35]

From photoelectron spectroscopy in air (PESA) measurement, we estimated the valence band maxima (VBM) of MAPbCl$_3$ to be −5.82 eV (Figure 2b). VBM of MAPbBr$_3$ and MAPbI$_3$ were previously measured to be −5.68 eV[36] and −5.43

eV,[37] respectively. The monotonic lowering of VBM in MAPbX$_3$ with descending halogen group (Cl to Br to I) is mainly due to the change of the halogen orbitals participating in the VBM from 3p to 4p to 5p, respectively, which leads to a more covalent bond between the halogen and lead ions.[38] From the VBM and the optical band gap we determined the conduction band edge position of MAPbCl$_3$ (Figure 2c).

As shown in Figure 3a we also studied recombination property of excitons by transient absorption (TA). We observed both fast ($\tau \sim 83$ ns) and slow ($\tau \sim 662$ ns) components of the carrier dynamics, as revealed from a biexponential fit of the TA signal. The fast and slow
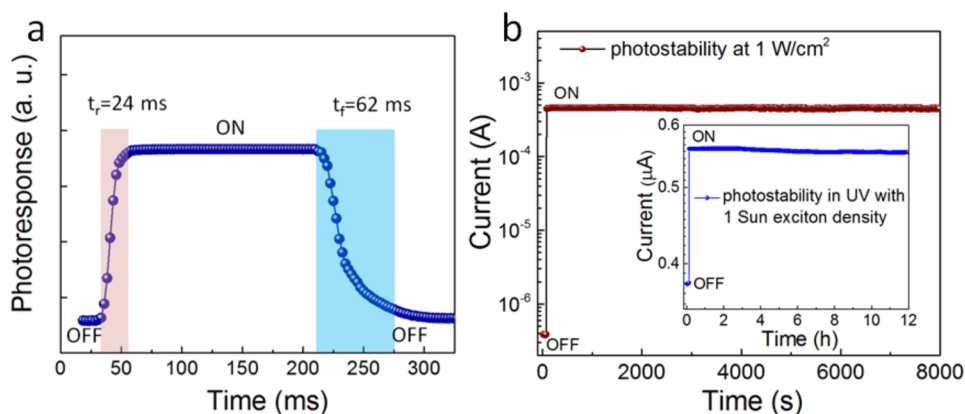
Figure 5. (a) Time dependent photoresponse. (b) photostability measured on the single crystal MAPbCl$_3$ photodetector in UV (1 W/cm^2), and inset represents data measured under UV light (1 sun excitation density).

components are likely associated with the surface and the bulk of the crystal, respectively. These values are comparable to the results presented for MAPbBr$_3$ and MAPbI$_3$ single crystals.[11,26]

We studied the charge-transport properties of MAPbCl$_3$ single crystal in order to evaluate its potential for optoelectronic applications. We formed a capacitor-like device with selective hole injection by sandwiching a MAPbCl$_3$ single crystal between two Pt electrodes deposited by sputtering, and investigated the evolution of space-charge-limited current (SCLC) under different biases (Figure 3b). At low electric field, an ohmic region is confirmed; we extracted the electrical conductivity (σ) to be 2.7×10^{-8} Ω^{-1} cm^{-1}. The $I-V$ characteristics of the crystal change at V_{TFL} (at 9.8 V) where the current exhibits a sharp rise ($I \alpha V^{n>3}$), indicating the transition into the trap-filled limit (TFL), where all the trap states are occupied by the charge carriers.[39] Exploiting the linear dependence between V_{TFL} and the trap density (n_{traps}),

$$n_{traps} = \frac{2\varepsilon\varepsilon_0 V_{TFL}}{eL^2}$$

where ε (23.9)[29] and ε_0 are the dielectric constant of MAPbCl$_3$ and the vacuum permittivity respectively, L is the thickness of the crystal and e is the elementary charge, we estimated the trap density n_{traps} to be $\sim 3.1 \times 10^{10}$ cm^{-3}. At higher bias, the current shows a quadratic dependence ($I \alpha V^2$). Fitting with the Mott–Gurney law,

$$J_d = \frac{9\varepsilon\varepsilon_0 \mu V^2}{8L^3}$$

where J_d is the current density and V is the applied voltage, we extracted the value of the carrier mobility (μ) as (42 ± 9) cm^2 V^{-1} s^{-1}. The uncertainties represent standard deviation in the measurements based on five similar devices. We also estimated the free charge carrier density $n_c = \sigma/e\mu$ to be $\sim 4 \times 10^9$ cm^{-3}.

Combining the μ value obtained from SCLC and the exciton lifetime τ by TA, we calculated diffusion length (L_D), which represents one of the key parameters for designing high-performance optoelectronic devices:

$$L_D = \sqrt{\frac{k_B T \mu \tau}{e}}$$

where k_B is the Boltzmann constant and T is the sample temperature. In particular, we estimated a best-case diffusion length (~ 8.5 μm) by using the longer carrier lifetime, namely

the bulk component, and a worst-case diffusion length (~ 3.0 μm) by considering the shorter carrier lifetime, ascribed to the surface of the crystal. All these results are comparable to the ones reported for the best-quality MAPbBr$_3$ and MAPbI$_3$ single crystals.[11,26]

As a prototypical demonstration of optoelectronic devices, we constructed a photodetector based on MAPbCl$_3$ single crystal, taking advantage of the materials large band gap and visible transparency. The device architecture is shown in Figure 4a. A semitransparent Pt layer of 20 nm (with transmittance of 26% at 365 nm) was deposited on the MAPbCl$_3$ perovskite crystal as the top electrode. A layer of 20 nm Ti/100 nm Au was deposited on the opposite side as the bottom electrode. The corresponding band energy diagram is illustrated in Figure 4b. To investigate the photoresponse, the current–voltage ($I-V$) curves of the device were measured in the dark and under illumination with 365 nm UV light (power intensity of 1 W/cm^2) as shown in Figure 4c. At 15 V, the photodetector showed a dark current as low as 4.15×10^{-7} A. Under light illumination, the photocurrent, particularly at high voltage bias, increases drastically, demonstrating a nonlinear and asymmetrical $I-V$ behavior. A photocurrent of 4.7×10^{-4} A was measured at an applied voltage of 15 V. In addition, a slight hysteresis behavior was observed under forward and reverse scans of bias (Figure S2, Supporting Information), which is consistent with the reports on other organo-lead halide perovskites, and it is likely due to the voltage-induced drift of ions.[40]

The temporal photoresponse measured at a bias voltage of 15 V is shown in Figure 4d. The current ON-OFF ratio was as high as 1.1×10^3. The responsivity (R) was calculated as follows,

$$R = \frac{I_{light} - I_{dark}}{P_{light}}$$

where I_{light} is the photocurrent (A), I_{dark} is the dark current (A), and P_{light} is the incident light power (W). At the bias voltage of 15 V, the responsivity of the MAPbCl$_3$ single crystal based photodetector was estimated to be 46.9 mA/W. Detectivity of 1.2×10^{10} Jones was calculated using the formula

$$D = \frac{R}{\sqrt{2qJ_{dark}}}$$

where q is the elementary charge and J_{dark} is the dark current density.

The response speed is another important parameter for photodetectors, which is related to the extraction of the photogenerated charge carriers. The thickness of the MAPbCl$_3$ single crystal was reduced to 350 μm in order to minimize parasitic resistance, which is the limit of our polishing technique (see Supporting Information for more details). The photo response as a function of time is shown in Figure 5a, demonstrating a rise time (t_r) of 24 ms and a decay time (t_f) of 62 ms. These response times compare favorably to those reported for UV photodetectors based on TiO$_2$ thin films (rise time: 6 s; decay time: 15 s)[41] and ZnO nanoparticles (rise time: 48 s; decay time: 0.9 s).[42]

Photostability of the MAPbCl$_3$ single crystal photodetector, without encapsulation, was studied at room temperature in ambient air with a humidity level of 55−60%. As illustrated in Figure 5b, at an applied bias of 15 V and under continuous 365 nm light illumination (1 W/cm^2), the photocurrent as a function of time remains stable up to 8000 s without degradation. The inset of Figure 5b demonstrates the photostability of the same device measure under blue light (1 Sun excitation density). These MAPbCl$_3$ single crystals present high photostability over 12 h. This exceptional device stability can be ascribed to the fact that our single crystal contains very few defects and is free from grain boundary (Figure S3, Supporting Information), which benefits the structural and chemical integrity of the device.

Perovskite-structured oxide single crystals like SrTiO$_3$,[43] LaAlO$_3$,[44] LiTaO$_3$[45] and LiNbO$_3$[46] as well as their hetero-structures[47−49] have been used in UV photodetectors. However, such oxide single crystals are quite expensive and cannot be easily produced in most laboratories. One important advantage of hybrid perovskite single crystals is their solution-based processability. As shown in Table S1 in the Supporting Information, our device based on hybrid perovskite single crystal is quite promising compared to those published in literature.

In summary, we have demonstrated a simple one step approach to grow high-quality MAPbCl$_3$ crystals through the proper selection of DMSO−DMF solution, which allowed the crystallization to occur in the retrograde solubility regime. The optical and electrical properties of the single crystal were studied; and band structure and charge transport parameters, such as carrier mobility and diffusion length, were determined. The grown MAPbCl$_3$ crystals possess optoelectronic properties that make them attractive candidate semiconductors for visible-blind UV photodetection. We found that MAPbCl$_3$ single crystal-based UV-photodetector provides high detectivity and ON-OFF ratio, with a response time in the order of milliseconds, indicating that hybrid perovskite single crystals are promising to function as the active component in such optoelectronic devices. In addition, the exceptional long-term stability in ambient conditions with 55% humidity suggests a potential for the deployment of MAPbCl$_3$ single crystals in practical applications.

■ ASSOCIATED CONTENT

Ⓢ Supporting Information

The Supporting Information is available free of charge on the ACS Publications website at DOI: 10.1021/acs.jpclett.5b01666.

Precursor materials and single crystal synthesis details. Details of all the characterization techniques. Solubility test details. Hysteresis in I−V characteristic and cross-sectional SEM image of single crystal. (PDF)

■ AUTHOR INFORMATION

Corresponding Authors
*E-mail: tao.wu@kaust.edu.sa.
*E-mail: osman.bakr@kaust.edu.sa.

Author Contributions
‖(G.M., A.D.S.) These authors contributed equally to this work.

Notes
The authors declare no competing financial interest.

■ REFERENCES

(1) Snaith, H. J. Perovskites: the emergence of a new era for low-cost, high-efficiency solar cells. (2013). *J. Phys. Chem. Lett.* **2013**, *4*, 3623−3630.

(2) Christians, J. A.; Fung, R. C. M.; Kamat, P. V. An inorganic hole conductor for organo-lead halide perovskite solar cells: Improved hole conductivity with copper iodide. *J. Am. Chem. Soc.* **2014**, *136*, 758−764.

(3) Liu, D.; Kelly, T. L. Perovskite solar cells with a planar heterojunction structure preparing using room-temperature solution processing techniques. *Nat. Photonics* **2013**, *8*, 133−138.

(4) Liang, K.; Mitzi, D. B.; Prikas, M. T. Synthesis and characterization of organic-inorganic perovskite thin films prepared using a versatile two-step dipping technique. *Chem. Mater.* **1998**, *10*, 403−411.

(5) You, J.; Hong, Z.; Yang, Y. (M.); Chen, Q.; Cai, M.; Song, T.-B.; Chen, C.-C.; Lu, S.; Liu, Y.; Zhou, H.; et al. Low-temperature solution-processed perovskite solar cells with high efficiency and flexibility. *ACS Nano* **2014**, *8*, 1674−1680.

(6) Noh, J. H.; Im, S. H.; Heo, J. H.; Mandal, T. N.; Seok, S., Il. Chemical management for colorful, efficient, and stable inorganic-organic hybrid nanostructured solar cells. *Nano Lett.* **2013**, *13*, 1764−1769.

(7) Kojima, A.; Teshima, K.; Shirai, Y.; Miyasaka, T. Organo metal halide perovskites as visible-light sensitizer for photovoltaic cells. *J. Am. Chem. Soc.* **2009**, *131*, 6050−6051.

(8) De Wolf, S.; Holovsky, J.; Moon, S.-J.; Löper, P.; Niesen, B.; Ledinsky, M.; Haug, F.-J.; Yum, J.-H.; Ballif, C. Organometallic halide perovskites: Sharp optical absorption edge and its relation to photovoltaic performance. *J. Phys. Chem. Lett.* **2014**, *5*, 1035−1039.

(9) Xing, G.; Mathews, N.; Sun, S.; Lim, S. S.; Lam, Y. M.; Grätzel, M.; Mhaisalkar, S.; Sum, T. C. Long-range balanced electron- and hole-transport lengths in organic-inorganic CH$_3$NH$_3$PbI$_3$. *Science* **2013**, *342*, 344−347.

(10) Wu, X.; Trinh, M. T.; Niesner, D.; Zhu, H.; Norman, Z.; Owen, J. S.; Yaffe, O.; Kudisch, B. J.; Zhu, X.-Y. Trap states in lead iodide perovskites. *J. Am. Chem. Soc.* **2015**, *137*, 2089−2096.

(11) Shi, D.; Adinolfi, V.; Comin, R.; Yuan, M.; Alarousu, E.; Buin, A.; Chen, Y.; Hoogland, S.; Rothenberger, A.; Katsiev, K.; et al. Low trap-state density and long carrier diffusion in organolead trihalide perovskite single crystals. *Science* **2015**, *347*, 519−522.

(12) Manser, J. S.; Kamat, P. V. Band filling with free charge carriers in organometal halide perovskites. *Nat. Photonics* **2014**, *8*, 737−743.

(13) Park, N.-G. Organometal perovskite light absorbers toward a 20% efficiency low-cost solid-state mesoscopic solar cell. *J. Phys. Chem. Lett.* **2013**, *4*, 2423−2429.

(14) Docampo, P.; Ball, J. M.; Darwich, M.; Eperon, G. E.; Snaith, H. J. Efficient organometal trihalide perovskite planar-heterojunction solar cells on flexible polymer substrates. *Nat. Commun.* 2013, *4*, 2761.

(15) Sheikh, A. D.; Bera, A.; Haque, M. A.; Rakhi, R. B.; Gobbo, S. D.; Alshareef, H. N.; Wu, T. Atmospheric effects on the photovoltaic performance of hybrid perovskite solar cells. *Sol. Energy Mater. Sol. Cells* 2015, *137*, 6−14.

(16) Wang, H.; Sheikh, A. D.; Feng, Q.; Li, F.; Chen, Y.; Yu, W.; Alarousu, E.; Ma, C.; Haque, M. A.; Shi, D.; Wang, Z. S.; Mohammed, O. F.; Bakr, O. M.; Wu, T. Facile synthesis and high performance of a new carbazole-based hole-transporting material for hybrid perovskite solar cells. *ACS Photonics* 2015, *2*, 849−855.

(17) Nie, W.; Tsai, H.; Asadpour, R.; Blancon, J. C.; Neukirch, A. J.; Gupta, G.; Crochet, J. J.; Chhowalla, M.; Tretiak, S.; Alam, M. A.; et al. High-efficiency solution-processed perovskite solar cells with milli-meter-scale grains. *Science* 2015, *347*, 522−525.

(18) Jaramillo-Quintero, O. A.; Sanchez, R. S.; Rincon, M.; Mora-Sero, I. Bright visible-infrared light emitting diodes based on hybrid halide perovskite with spiro-ometad as a hole-injecting layer. *J. Phys. Chem. Lett.* 2015, *6*, 1883−1890.

(19) Tan, Z. K.; Moghaddam, R. S.; Lai, M. L.; Docampo, P.; Higler, R.; Deschler, F.; Price, M.; Sadhanala, A.; Pazos, L. M.; Credgington, D.; et al. Bright light-emitting diodes based on organometal halide perovskite. *Nat. Nanotechnol.* 2014, *9*, 687−692.

(20) Wehrenfennig, C.; Liu, M.; Snaith, H. J.; Johnston, M. B.; Herz, L. M. Homogeneous Emission Line Broadening in the Organo Lead Halide Perovskite CH$_3$NH$_3$PbI$_{3-x}$Cl$_x$. *J. Phys. Chem. Lett.* 2014, *5*, 1300−1306.

(21) Xing, G.; Mathews, N.; Lim, S. S.; Yantara, N.; Liu, X.; Sabba, D.; Grätzel, M.; Mhaisalkar, S.; Sum, T. C. Low-temperature solution-processed wavelength-tunable perovskites for lasing. *Nat. Mater.* 2014, *13*, 476−480.

(22) Guo, Y.; Liu, C.; Tanaka, H.; Nakamura, E. Air-stable and solution-processable perovskite photodetectors for solar-blind UV and visible light. *J. Phys. Chem. Lett.* 2015, *6*, 535−539.

(23) Chen, H. W.; Sakai, N.; Jena, A. K.; Sanehira, Y.; Ikegami, M.; Ho, K. C.; Miyasaka, T. A Switchable high-sensitivity photodetecting and photovoltaic device with perovskite absorber. *J. Phys. Chem. Lett.* 2015, *6*, 1773−1779.

(24) Dou, L.; Yang, Y. M.; You, J.; Hong, Z.; Chang, W.-H.; Li, G.; Yang, Y. Solution-processed hybrid perovskite photodetectors with high detectivity. *Nat. Commun.* 2014, *5*, 5404.

(25) Dong, Q.; Fang, Y.; Shao, Y.; Mulligan, P.; Qiu, J.; Cao, L.; Huang, J. Electron-hole diffusion lengths > 175 μm in solution-grown CH$_3$NH$_3$PbI$_3$ single crystals. *Science* 2015, *347*, 967−970.

(26) Saidaminov, M. I.; Abdelhady, A. L.; Murali, B.; Alarousu, E.; Burlakov, V. M.; Peng, W.; Dursun, I.; Wang, L.; He, Y.; Maculan, G.; et al. High-quality bulk hybrid perovskite single crystals within minutes by inverse temperature crystallization. *Nat. Commun.* 2015, *6*, 7586.

(27) Dang, Y.; Liu, Y.; Sun, Y.; Yuan, D.; Liu, X.; Lu, W.; Liu, G.; Xia, H.; Tao, X. Bulk crystal growth of hybrid perovskite material CH$_3$NH$_3$PbI$_3$. *CrystEngComm* 2015, *17*, 665−670.

(28) Maeda, M.; Hattori, M.; Hotta, A.; Suzuki, I. Dielectric studies on CH$_3$NH$_3$PbX$_3$ (X = Cl and Br) single crystals. *J. Phys. Soc. Jpn.* 1997, *66*, 1508−1511.

(29) Poglitsch, A.; Weber, D. Dynamic disorder in methylammo-niumtrihalogenoplumbates (II) observed by millimeter-wave spectros-copy. *J. Chem. Phys.* 1987, *87*, 6373−6378.

(30) Xu, Q.; Eguchi, T.; Nakayama, H.; Nakamura, N.; Kishita, M. Molecular motions and phase transitions in solid CH$_3$NH$_3$PbX$_3$ (x = Cl, Br, I) as studied by NMR and NQR. *Z. Naturforsch., A: Phys. Sci.* 1991, *46*, 240−246.

(31) Mashiyama, H.; Kurihara, Y.; Azetsu, T. Disordered cubic perovskite structure of CH$_3$NH$_3$PbX$_3$ (X = Cl, Br, I). *J. Korean Phys. Soc.* 1998, *32*, 156−158.

(32) Taylor, P. A. Purification techniques and analytical methods for gaseous and metallic impurities in high-purity silane. *J. Cryst. Growth* 1988, *89*, 28−38.

(33) Baikie, T.; Barrow, N. S.; Fang, Y.; Keenan, P. J.; Slater, P. R.; Piltz, R. O.; Gutmann, M.; Mhaisalkar, S. J.; White, T. J. A combined single crystal neutron/X-ray diffraction and solid-state nuclear magnetic resonance study of the hybrid perovskites CH$_3$NH$_3$PbX$_3$ (X = I, Br and Cl). *J. Mater. Chem. A* 2015, *3*, 9298−9307.

(34) Kitazawa, N.; Watanabe, Y.; Nakamura, Y. Optical properties of CH$_3$NH$_3$PbX$_3$ (X = halogen) and their mixed-halide crystals. *J. Mater. Sci.* 2002, *37*, 3585−3587.

(35) D'Innocenzo, V.; Srimath Kandada, A. R. S.; De Bastiani, M.; Gandini, M.; Petrozza, A. Tuning the light emission properties by band gap engineering in hybrid lead halide perovskite. *J. Am. Chem. Soc.* 2014, *136*, 17730−17733.

(36) Ryu, S.; Noh, J. H.; Jeon, N. J.; Kim, Y. C.; Yang, W. S.; Seo, J.; Seok, S., Il. Voltage output of efficient perovskite solar cells with high open-circuit voltage and fill factor. *Energy Environ. Sci.* 2014, *7*, 2614−2618.

(37) Kim, H. S.; Lee, C.-R.; Im, J. H.; Lee, K. B.; Moehl, T.; Marchioro, A.; Moon, S. J.; Humphry-Baker, R.; Yum, J. H.; et al. Lead iodide perovskite sensitized all-solid-state submicron thin film mesoscopic solar cell with efficiency exceeding 9%. *Sci. Rep.* 2012, *2*, 1−7.

(38) Huang, L. Y.; Lambrecht, W. R. L. Electronic band structure, phonons, and exciton binding energies of halide perovskites CsSnCl$_3$, CsSnBr$_3$, and CsSnI$_3$. *Phys. Rev. B: Condens. Matter Mater. Phys.* 2013, *88*, 1−12.

(39) Lampert, M. A.; Mark, P. *Current Injection in Solids*; Academic Press: New York, 1970.

(40) Xiao, Z.; Yuan, Y.; Shao, Y.; Wang, Q.; Dong, Q.; Bi, C.; Sharma, P.; Gruverman, A.; Huang, J. Giant switchable photovoltaic effect in organometal trihalide perovskite devices. *Nat. Mater.* 2014, *14*, 193−198.

(41) Xue, H.; Kong, X.; Liu, Z.; Liu, C.; Zhou, J.; Chen, W.; Ruan, S.; Xu, Q. TiO$_2$ based metal-semiconductor-metal ultraviolet photo-detectors. *Appl. Phys. Lett.* 2007, *90*, 201118.

(42) Jun, J. H.; Seong, H.; Cho, K.; Moon, B. M.; Kim, S. Ultraviolet photodetectors based on ZnO nanoparticles. *Ceram. Int.* 2009, *35*, 2797−2801.

(43) Xing, J.; Zhao, K.; Lu, H. B.; Wang, X.; Liu, G. Z.; Jin, K. J.; He, M.; Wang, C. C.; Yang, G. Z. Visible-blind, ultravioletsensitive photodetector based on SrTiO$_3$ single crystal. *Opt. Lett.* 2007, *32*, 2526−2528.

(44) Xing, J.; Guo, E. J.; Jin, K. J.; Lu, H. B.; Wen, J.; Yang, G. Z. Solar-blind deep-ultraviolet photodetectors based on an LaAlO$_3$ single crystal. *Opt. Lett.* 2009, *34*, 1675−1677.

(45) Guo, E. J.; Xing, J.; Jin, K. J.; Lu, H. B.; Wen, J.; Yang, G. Z. Photoelectric effects of ultraviolet fast response and high sensitivity in LiNbO$_3$ single crystal,. *J. Appl. Phys.* 2009, *106*, 023114.

(46) Guo, E. J.; Xing, J.; Lu, H. B.; Jin, K. J.; Wen, J.; Yang, G. Z. Ultraviolet fast-response photoelectric effects in LiTaO$_3$ single crystal. *J. Phys. D: Appl. Phys.* 2010, *43*, 015402.

(47) Bera, A.; Peng, H.; Lourembam, J.; Shen, Y.; Sun, X. W.; Wu, T. A versatile light-switchable nanorod memory: wurtzite ZnO on perovskite SrTiO$_3$. *Adv. Funct. Mater.* 2013, *23*, 4977−4984.

(48) Luo, C.; Jin, K. X.; Chen, C. L.; Wu, T. Suppression of photovoltaic effect by magnetic field in Pr$_{0.65}$(Ca$_{0.75}$Sr$_{0.25}$)$_{0.35}$MnO$_3$/Nb:SrTiO$_3$ heterostructure. *Appl. Phys. Lett.* 2013, *103*, 212401.

(49) Jin, K. X.; Zhai, Y. X.; Li, H.; Tian, Y. F.; Luo, B. C.; Wu, T. Favorable ultraviolet photoelectric effects in TbMnO$_3$/Nb-SrTiO$_3$ heterostructures. *Solid State Commun.* 2014, *199*, 39−42.